Prediction of electronic (hyper)polarizabilities of titania nanotubes: A DFT periodic study

ARTICLE *in* COMPUTATIONAL MATERIALS SCIENCE · FEBRUARY 2013

Impact Factor: 2.13 · DOI: 10.1016/j.commatsci.2012.11.002

3 AUTHORS:

Anna Maria Ferrari
Università degli Studi di Torino
88 PUBLICATIONS **2,703** CITATIONS
SEE PROFILE

Martina Lessio
Princeton University
8 PUBLICATIONS **13** CITATIONS
SEE PROFILE

Michel Rérat
Université de Pau et des Pays de l'Adour
135 PUBLICATIONS **1,918** CITATIONS
SEE PROFILE

Computational Materials Science 68 (2013) 280–286

Contents lists available at SciVerse ScienceDirect

Computational Materials Science

journal homepage: www.elsevier.com/locate/commatsci

Prediction of electronic (hyper)polarizabilities of titania nanotubes: A DFT periodic study

Anna Maria Ferrari [a,*], Martina Lessio [a], Michel Rérat [b]

[a] Dipartimento di Chimica IFM, Università di Torino and NIS – Nanostructured Interfaces and Surfaces, Centre of Excellence, Via P. Giuria 7, 10125 Torino, Italy[1]
[b] Equipe de Chimie Physique, IPREM UMR5254, Université de Pau et des Pays de l'Adour, FR-64000 Pau, France

ARTICLE INFO

Article history:
Received 1 September 2012
Received in revised form 28 October 2012
Accepted 2 November 2012
Available online 7 December 2012

Keywords:
Nanostructures
Ab initio calculations
Dielectric properties

ABSTRACT

In this work, the static electronic (hyper)polarizabilities of $(0,n)$ and $(n,0)$ lepidocrocite nanotubes have been computed for the first time using the coupled perturbed Kohn Sham (CPKS) scheme recently implemented in the CRYSTAL code. The dependence of the response properties of the 1D-systems to electric field on the choice of the basis set and density functional has been critically analyzed. Results obtained by fit at the infinite diameter limit are compared to those of the lepidocrocite flat sheet.

1. Introduction

In recent years a great interest has been devoted to titanium dioxide because of its wide range of applications in many scientific and industrial fields [1]. Such applications include as solar cells, photocatalytic decomposition of organic material [2], photoelectrochemical splitting of water [3], gas sensors [4] and electrodes for lithium batteries [5]. Specific applications critically depend on the crystalline phase and structure of the TiO_2 because they affect many properties of the material. Presently, the most investigated phases number three: rutile, anatase and lepidocrocite. Rutile and anatase exist both as bulk and nanostructured phase. Lepidocrocite exists only as a nanostructured system, in particular as a thin film synthesized on a metal surface or as a nanotube. In particular, the latter structure has been the object of both experimental characterization and ab initio calculations. SAED and HRTEM studies performed by Wang have demonstrated that nanotubes prepared from anatase powder have the anatase layer structure. Saponjic has demonstrated through XANES spectra that materials so prepared exhibit quasi-anatase structure [6,7]. However, more recent electron diffraction studies conducted by Akita proved that nanotube samples prepared in a similar way have a lepidocrocite-like crystalline structure [8]. This experimental observation is supported by ab initio calculations on thin, anatase-derived nanolayers, in which the nanolayers are shown to rearrange spontaneously to lepidocrocite [9].

As a consequence, growing attention has been dedicated to TiO_2 nanotubes with lepidocrocite-like crystal structures. Up to now, research work has principally investigated the stability and electronic properties of these systems and their dependence on the size of the nanostructures (diameter of the tubes) [10–13]. However, the dielectric properties of these materials remain uninvestigated, despite their relevance to their separation, alignment and electric field manipulations. The properties are also required for analyzing Raman spectra, optical excitations, screening at contacts and plasma in nanotube arrays [14]. By understanding the relationship between crystalline and geometric features of these systems and their dielectric properties, it is possible to gain knowledge useful to improving their performance in specific applications.

In this work, the high frequency (i.e. electronic) static polarizability (α) and first (β) and second (γ) hyperpolarizability tensors of $(n,0)$ and $(0,n)$ lepidocrocite nanotubes, LNTs, have been computed, Fig. 1. The coupled perturbed Kohn–Sham (CPKS) scheme, implemented in the periodic CRYSTAL [15] code, has been employed for all calculations. See Refs. [16,17] for a detailed description of this method. The computational scheme is self-consistent and very efficient. Tubes as large as (48,0) and containing 288 atoms in the unit cell, could have been investigated with a medium size basis set and a severe set up of computational parameters. This has permitted the study of the dependence of the optical dielectric properties on the nanotube radius and the morphology of the tubes (rolling directions) with reference to the limiting case of a lepidocrocite monolayer. This work is a first report concerning the calculations of dielectric properties of TiO_2 nanotubes.

* Corresponding author.
E-mail address: anna.ferrari@unito.it (A.M. Ferrari).
[1] http://www.nis.unito.it.

0927-0256/$ - see front matter © 2012 Elsevier B.V. All rights reserved.
http://dx.doi.org/10.1016/j.commatsci.2012.11.002

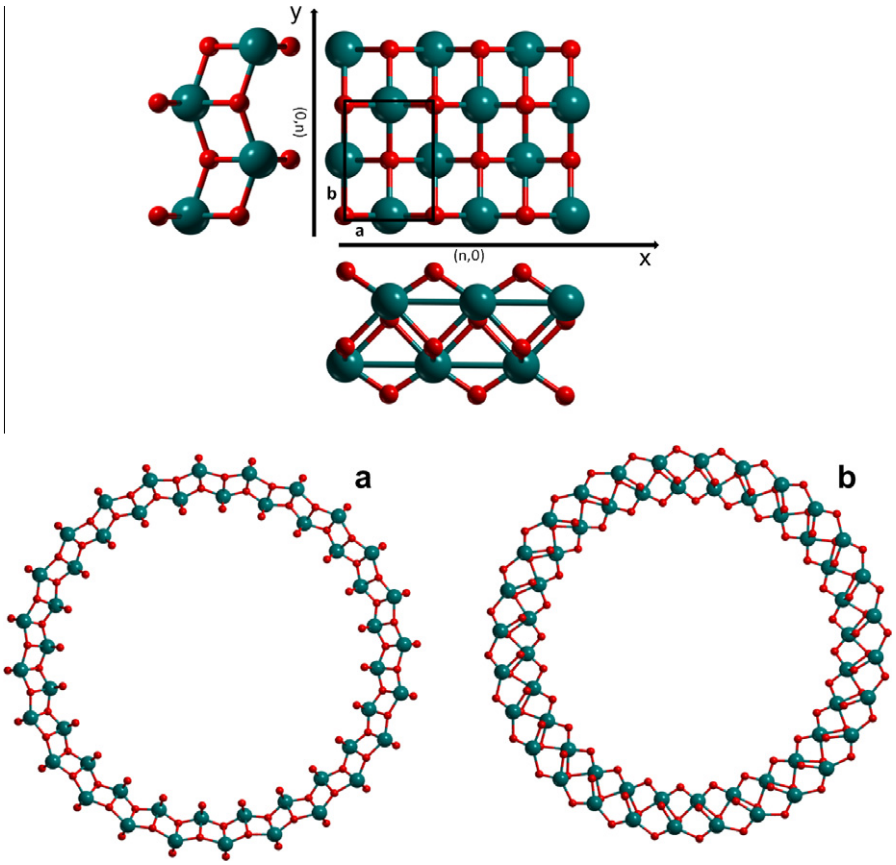

Fig. 1. Rolling up of lepidocrocite nanotubes: $(n,0)$ nanotubes supercell is built by rolling up along the direction of the cell parameter a which corresponds to the x axis, whereas $(0,n)$ nanotubes supercell is built by rolling up along the direction of the cell parameter b which corresponds to the y axis. Side view of: (a) (0,24) and (b) (28,0) lepidocrocite nanotube titanium atoms in blue, oxygen atoms in red. (For interpretation of the references to colour in this figure legend, the reader is referred to the web version of this article.)

2. Computational details

Calculations were performed with a development version of the periodic ab initio CRYSTAL09 code [15], within a DFT scheme. Reference calculations for the lepidocrocite monolayer were performed by employing different functionals and basis sets of increasing size. A1 is a medium size basis set already used in previous TiO_2 nanotube calculations. It comprises an all-electron 8-411G (d) gaussian-type basis set [18] for O atoms, and a Hay–Wadt (HW) small core ECP [19] with a 411-31 [3sp2d] basis set for valence electrons for Ti atoms. Basis set B1 is based on the TZV-P (for Ti) and TZ-P (for O) Ahlrichs all-electron basis sets [20], namely a 511111-411-1 [6s3p1d] Gaussian-type basis set for O and a 84211-6311-411[5s4p3d] for Ti atoms. The B2-5 basis set differs from B1 by the presence of additional polarization function: an f function on Ti ($\alpha_f = 0.562$) in added in B2. The PP polarization (2d1f) set is added to O atoms in basis set B3. B4 is the combination of B2 and B3. In B5 the PPP polarization (3d2f) set is added to O atoms together with the presence of two f functions on Ti ($\alpha_f = 1.075, 0.339$). Basis set C1 is composed of the B5 set for O and a pruned QZV-(2f) -resulting in details as 11 41111111-94111-311-2 [9s5p3d2f]- for Ti.

The pure DFT PBE and the hybrid PBE0 [21] and B3LYP functionals have been considered. In addition, the dependence of the dielectric properties on the amount of exact exchange incorporated into the hybrid functional, has been tested by considering PBE-Fx functionals derived from PBE0. In these functionals different percentages, x, of exact exchange have been included, namely $x = 20$ (PBE-F20), $x = 12.5$ (PBE-F12) and $x = 6$ (PBE-F6).

In the CRYSTAL code, the level of accuracy in evaluating the Coulomb and the exchange integrals is controlled by five parameters T ($T1$, $T2 = T1$, $T3 = T1$, $T4$, $T5 = 2T4$). The reciprocal space is sampled according to a regular sublattice determined by the shrinking factor S [15]. Reference calculations have been performed with different selections of the integrals selection parameters and different sampling of the reciprocal space. Results are reported in Tables S1 and S2 of Supplementary Materials. Inspection of the computed data indicates that the two parameters controlling the exchange series ($T4$ and $T5$) appear to be critical and must be set to large values of $T5$ ($T5 \geqslant 70$); On the other hand, the parameters controlling the Coulomb series, once fixed at least at $T1 \geqslant 7$, do not significantly affect the computed properties for. Then, the selection of T (7,7,7,35,70) has been adopted for nanotube calculations.

The DFT exchange–correlation energy is evaluated by numerical integration over the unit cell volume. In CRYSTAL, a Gauss–Legendre radial and a Lebedev angular grid of points is used. In the present calculations, a (75,974) pruned grid is applied. The convergence threshold for SCF energy was set to 10^{-10} Ha.

Dielectric properties have been computed for the equilibrium structures (cell and atomic coordinates) obtained at the PBE0/A1 level and widely described in previous works [11,13].

3. Results and discussion

3.1. The lepidocrocite nanosheet

Lepidocrocite nanosheets are the most stable titania phase at the monolayer limit. They do not exist as self-standing material but only when supported on metal substrates or in nanostructures such as nanotubes. Indeed, the lepidocrocite polymorphs have

been reported to be most widely observed in titania nanotubes. Lepidocrocite sheets derive from an anatase (0 0 1) bilayer. The film is not stable in the bulk-like structure and undergoes a spontaneous transformation in which the upper part of the film glides over the lower part along the direction of the surface two-coordinated oxygen chains. The resulting lepidocrocite structure is more stable than the initial structure by 0.16 eV per TiO_2 unit (PBE0/A1 result) and is characterized by a more contracted primitive rectangular unit cell (a = 3.77 Å and b = 3.01 Å). This result agrees with previous calculations [9,13]. The higher stability of lepidocrocite films is related to the presence of bulk-like six-coordinated Ti opposed to the five-coordinated Ti atoms present in the (0 0 1) bilayer. The electronic structure of lepidocrocite and anatase are similar except for a difference in the band gap: the lepidicrocite band gap is about 15% larger than the anatase one regardless of the computational approach employed. To our knowledge, there is only one report on dielectric properties of lepidocrocite nanosheet. In this work, only the α tensor was computed and only the PBE functional was employed [22]. Thus, in order to provide critical background to the selected set up of computational parameters, the (hyper)polarizabilities have been computed by employing several basis sets and functionals. These results are reported in Tables 1 and 2 and S3 and S4 of Supplementary materials.

The parallel component of the polarizability α_{xx} and α_{yy} (x and y axes are oriented along the a and b lattice vectors, respectively) are not equivalent per symmetry; all the components of the first hyperpolarizability tensor β are zero due to the presence of an inversion centre in the lepidocrocite sheet. The nonzero components of the γ tensor are γ_{xxxx}, γ_{yyyy}, γ_{zzzz}, γ_{xxyy}, γ_{xxzz} and γ_{yyzz}.

Table 1 shows the dependence of the (hyper)polarizability components on the extension of the basis set. Inclusion of polarization functions in the basis set appears to be of crucial importance. For instance, the inclusion of a f function on Ti (basis set B2) modifies α_{xx} and α_{yy} by 5–10% whereas further extension of the basis set by additional polarization functions on O (from the P to PP set, basis set B4) does not yield significant variations. Much more critical is the basis set dependence of the γ tensor components. For instance, γ_{xxxx} varies by 40% from B1 to B2. The addition of the PP polarization set on O increases γ_{xxxx} by 50% (B4), and by another 50% more than B4 with the PPP set on O and a second f function on Ti (B5). A further increase in the size of the basis set (C1) produces minor changes in the γ values (the variation of the more sensitive components is less than 10%). In the same way as for PBE0, a strong dependence on the basis set size is observed in B3LYP calculations (Table S4) whereas a much faster convergence with respect to the size of the basis set has been found in the case of PBE results (Table S3).

Calculation of the dielectric properties have been shown to depend significantly on the choice of the basis set: moving from the smallest (A1) to the largest (C1) basis set the most sensitive γ components vary up to 50%. However, we can note a semiquantitative agreement between the predictions by the two basis sets, as the relative order of magnitude of γ values is always preserved. For this reason, only A1 has been adopted in the following study of the lepidocrocite nanotubes since the large unit cell of these latter systems leading to huge computational demand makes the use of larger basis sets prohibitive.

Table 2
Dependence of the lepidocrocite monolayer dielectric properties on the amount of exchange (a_x) incorporated in the hybrid functional (F). The choice of functionals ranges from the standard PBE0 (a_x = 25%) to PBE (a_x = 0%); intermediate cases, PBE-F20, PBE-F12 and PBE-F6 are characterized by a_x = 20%, 12% and 6%, respectively. Energy gap (E_g) in eV, polarizability (α) in au per TiO_2 unit which are equivalent to 1649E−41 (C^2m^2)/J; second hyperpolarizability (γ) in au per TiO_2 unit which are equivalent to 6235E−65 (C^4m^4)/J^3. Cell parameters (a = 3.03, b = 3.71 Å) from PBE0/A1 results. All calculations at the F/A1//PBE0/A1 level, T (8,8,8,50,100) and S = 12. See text for details.

F	PBE0	PBE-F20	PBE-F12	PBE-F6	PBE	B3LYP
E_g	5.53	5.02	4.25	3.68	3.14	5.04
α_{xx}	94	97	103	108	114	97
α_{yy}	62	64	69	74	79	63
α_{zz}	13	13	13	13	13	13
γ_{xxxx}	−7276	−2186	15,612	38,931	79,500	-2821
γ_{xxyy}	−289	1612	7224	14,848	28,607	1182
γ_{xxzz}	1475	1581	1735	1898	2140	1586
γ_{yyyy}	77,043	95,915	140,616	196,110	289,127	93,447
γ_{yyzz}	556	644	780	936	1162	616
γ_{zzzz}	24	24	29	28	30	23

In Table 2 the dielectric properties computed with PBE and hybrid methods are reported. First of all, the methods predict a large anisotropy of the polarizability tensor: the components corresponding to the periodic directions (α_{xx} and α_{yy}) are not equivalent (differ by more than 30%) and are several times larger than α_{zz} (along the non-periodic direction).

Computed α values vary significantly with the choice of functional. An inverse correlation is clearly observed between the α tensor components and the computed band gap of lepidocrocite. The reported band gap decreases as the amount of exact exchange (a_x) incorporated in the functional decreases. Specifically, the order PBE0 > PBE-F20 ≈ B3LYP > PBE-F12 > PBE-F6 > PBE is observed. This is not unexpected because the polarizability is determined by the response of the electronic structure to the electric field perturbation and depends on the asymptotic behaviour of the exchange–correlation potential v_{xc}. Additionally, the band gap is directly involved in the expression of the polarizability (see Refs. [16,17] for details). Energy level differences appear in the denominator, thus lowering the polarizability when the energy gap increases. Unlike the PBE functional, PBE derived hybrids reduce the self-interaction error and partially recover the correct asymptotic behaviour of v_{xc}. Notice, in addition, that the band gap is substantially independent of the basis set size, Table 1, justifying the

Table 1
Basis set (X) dependence of dielectric properties of the lepidocrocite monolayer: energy gap (E_g) in electronvolt (eV), polarizability (α) in au per TiO_2 unit which are equivalent to 1649E−41 (C^2m^2)/J; second hyperpolarizability (γ) in au per TiO_2 unit which are equivalent to 6235E−65 (C^4m^4)/J^3. All calculations at the PBE0/X//PBE0/A1 level; T = (8,8,8,50,100) and S = 12. See text for details.

X		A1	B1	B2	B3	B4	B5	C1
Basis set	Ti	HW-3sp2d	5s4p3d	5s4p3d-1f	5s4p3d	5s4p3d-1f	5s4p3d-2f	9s5p3d-2f
	O	8–411G(d)	6s3p-1d	6s3p-1d	6s3p-2d1f	6s3p-2d1f	6s3p-3d2f	6s3p-3d2f
E_g		5.53	5.25	5.40	5.29	5.40	5.39	5.43
α_{xx}		94	104	99	102	99	99	98
α_{yy}		62	64	62	67	65	66	66
α_{zz}		13	13	13	13	13	–	–
γ_{xxxx}		−7276	−26,530	−16,584	−12,133	−6569	−3903	−3682
γ_{xxyy}		−289	1013	991	601	796	739	562
γ_{xxzz}		1475	1782	1680	1608	1542	1540	1539
γ_{yyyy}		77,043	91,556	85,187	91,992	86,987	87,751	86,700
γ_{yyzz}		556	660	628	632	610	606	589
γ_{zzzz}		24	46	48	40	46	54	59

moderate dependence of α tensor on selected basis set. Determining which method provides better results is not a simple task. Comparison with observations cannot be used due to the lack of experimental data on lepidocrocite. The polarizability tensor has therefore been computed for anatase and results reported in Table S5. 12% of exact exchange is required for correct prediction of the anatase band gap. However, this small amount of exact exchange would lead to a worse long-range decay of v_{xc}. Indeed, a better estimate of the band gap is not necessarily combined with a better prediction of the α tensor. In fact, the better agreement with experiment is achieved by employing PBE0 and B3LYP with a percentage of $a_x \geqslant 20\%$. Notice however that the comparison is not straightforward since it is affected by various sources of nonnegligible errors associated for instance to the experimental techniques or to the sample features, such as for examples a polycrystalline structure.

An even larger dependence on DFT functionals can be recognized in the computed components of the γ tensor, Table 2. In particular the components involving periodic directions show a dramatic dependence on the amount of exact exchange incorporated in the functional. For instance γ_{yyyy} increases by a factor 4 from PBE0 to PBE, γ_{xxxx} by a factor 10 and γ_{xxyy} by a factor 100. Even a change of sign is observed for γ_{xxxx} that becomes negative when $a_x \geqslant 20\%$. Much less dramatic are the variations of the γ components involving non-periodic directions: in this case fluctuations never exceed a factor 2. In addition, it is possible to underline the large anisotropy of γ tensor: for instance the $\gamma_{xxxx}/\gamma_{yyyy}$ ratio is larger than 10 with all the hamiltonians considered in this work. Assessing which one is the most appropriate computational approach is not a simple issue for several reasons: (i) the scarce experience in hyperpolarizability calculations in the solid state, (ii) even scarcer experience when nanostructured materials are involved, and (iii) lack of experimental data. Nonetheless, accurate calculations carried out on molecular systems give the indication that functionals with $a_x = 20$–25%, namely PBE0 and B3LYP, provide accurate γ predictions, often comparable with CCSD(T) values [23–25]. Following this indication, even if derived from calculations on small molecules (the only available), the PBE0 functional has been considered for prediction of the nanotubes dielectric properties.

3.2. The lepidocrocite nanotubes

Both $(n,0)$ and $(0,n)$ nanotubes have been built from the lepidocrocite film, see Fig. 1. Details about their construction, morphology, relative stability and electron properties have been largely discussed in previous works [11–13]. The polarizability and second hyperpolarizability components have been computed on fully relaxed structures (cell parameter and atomic coordinates) and collected in Table 3. In the case where x is chosen as the periodic direction of the nanotubes, the independent (hyper)polarizability components are: α_{xx}, $\alpha_{yy} = \alpha_{zz}$, γ_{xxxx}, $\gamma_{yyyy} = \gamma_{zzzz} = 3\gamma_{yyzz}$ and $\gamma_{xxyy} = \gamma_{xxzz}$. All the other components as well as the whole first hyperpolarizability β tensor are equal to zero for symmetry reason.

When the tube becomes large and its surface flat, it can be shown that its (hyper)polarizability components are related to those of the monolayer. For $(0,n)$ tubes for which the periodic direction x corresponds to the lattice vector b of the lepidocrocite unit cell, we have at the infinite radius limit:

$$\begin{cases} \alpha_{xx}^{nanotube} = \alpha_{xx}^{layer} \\ \alpha_{yy}^{nanotube} = \alpha_{zz}^{nanotube} = \frac{1}{2}\left(\alpha_{yy}^{layer} + \alpha_{zz}^{layer}\right) \end{cases}$$
$$\begin{cases} \gamma_{xxxx}^{nanotube} = \gamma_{xxxx}^{layer} \\ \gamma_{yyyy}^{nanotube} = \frac{3}{8}\left(\gamma_{yyyy}^{layer} + \gamma_{zzzz}^{layer} + 2\gamma_{yyzz}^{layer}\right) \\ \gamma_{xxzz}^{nanotube} = \frac{1}{2}\left(\gamma_{xxyy}^{layer} + \gamma_{xxzz}^{layer}\right) \end{cases} \quad (1)$$

For $(n,0)$ tubes for which x corresponds to the lattice vector a of the lepidocrocite unit cell, we have:

$$\begin{cases} \alpha_{xx}^{nanotube} = \alpha_{yy}^{layer} \\ \alpha_{yy}^{nanotube} = \alpha_{zz}^{nanotube} = \frac{1}{2}\left(\alpha_{xx}^{layer} + \alpha_{zz}^{layer}\right) \end{cases}$$
$$\begin{cases} \gamma_{xxxx}^{nanotube} = \gamma_{yyyy}^{layer} \\ \gamma_{yyyy}^{nanotube} = \gamma_{zzzz}^{nanotube} = \frac{3}{8}\left(\gamma_{xxxx}^{layer} + \gamma_{zzzz}^{layer} + 2\gamma_{xxzz}^{layer}\right) \\ \gamma_{xxzz}^{nanotube} = \gamma_{xxyy}^{nanotube} = \frac{1}{2}\left(\gamma_{xxyy}^{layer} + \gamma_{yyzz}^{layer}\right) \end{cases} \quad (2)$$

Computed data for $(n,0)$ and $(0,n)$ nanotubes, along with their limit at infinite nanotube radius calculated value according to the above relations 1 and 2, are reported in Table 4. In addition, the longitudinal ($\alpha^{\parallel}$) and transverse ($\alpha^{\perp}$) polarizabilities of the $(n,0)$ and $(0,n)$ nanotubes per TiO_2 unit as well as their longitudinal ($\alpha'^{\parallel}$) and transverse ($\alpha'^{\perp}$) polarizabilities per unit length as function of the tube diameter D are plotted in Fig. 2. A size-independent behaviour of $\alpha^{\parallel}$ is observed for D larger than 30 Å, whatever is the chirality of the tubes and $\alpha^{\parallel}$ becomes rapidly constant with respect to D approaching the values of the lepidocrocite film. Consequently, in the range of D explored in this work (and for $D > 30$ Å), $\alpha'^{\parallel}$ is expected to be rather linear with respect to D, since the number of TiO_2 increases linearly with D (check values in Table 3). Chirality does not affect the trend with respect to D and the curves of $\alpha'^{\parallel}$ obtained for the $(n,0)$ and $(0,n)$ nanotubes are almost parallel: the difference are related to the anisotropy of the polarizability in the flat sheet. For $\alpha^{\perp}$ and $\alpha'^{\perp}$ the convergence with respect to D is far to be reached, has shown by Fig. 2. The presence of wiggles, more evident in the case of small nanotubes ($D < 30$ Å), is related to the mechanical strain in these systems as the interatomic distances are considerably deformed with respect to the flat sheet [11].To better understand the dependence of polarizability on D, $\alpha'^{\parallel}$ and $\alpha'^{\perp}$ have been fitted with both linear ($f(x) = a + bx$) and quadratic ($g(x) = a + bx + cx^2$) functions. Results of the fitting procedure, reported in the insert of Fig. 2, indicate that, although the numerical accuracy provided by the two curves is comparable (compare st. dev.), the c coefficient in $g(x)$ is at least one order of magnitude smaller than b, thus showing a larger weight of the linear term. However, it must be underlined that the limited number of points in the fitting scheme and the narrow range of explored D do not allow any definitive conclusions. In this context and with this awareness, we only assume a reasonable "linear" trend of $\alpha'^{\parallel}$ and $\alpha'^{\perp}$ with D (in the explored range).

The "linear" behaviour of $\alpha'^{\parallel}$ and $\alpha'^{\perp}$ resembles that of a thin dielectric cylindrical shell. Because the number of TiO_2 units per unit length is proportional to D, this result indicates that electrons are tightly bound to the nuclei and that every atom has almost the same polarizability in tubes of different size as would be the case for insulators. From the trend of alpha-components with respect to the size of the nanotube, the behaviour of LNTs appears similar to the case of BN nanotubes and dissimilar to the behaviour of carbon nanotubes [26]. In this latter case, it has been shown that both longitudinal and transversal polarizability components per carbon atom are linear with respect to D leading to a quadratic behaviour of the polarizability per unit length [27], due to the metallic character of graphene.

To better understand the dielectric properties of LNTs, an external electric field F_{out} has been applied along a transverse direction and the resulting electric field has been calculated along this direction going through the centre of the tube, Fig. 3. Inspection of the figure clearly shows that: (i) the electric field F_{ins} inside the tubes is uniform and slightly screened; (ii) the screening factor is dependent on the size of the tube; and (iii) the screening factor is 1.3–1.4 and 1.6–1.7 for $(0,n)$ and $(n,0)$ LNTs, respectively. This behaviour is qualitatively similar to that reported in the case of BN and C nano-

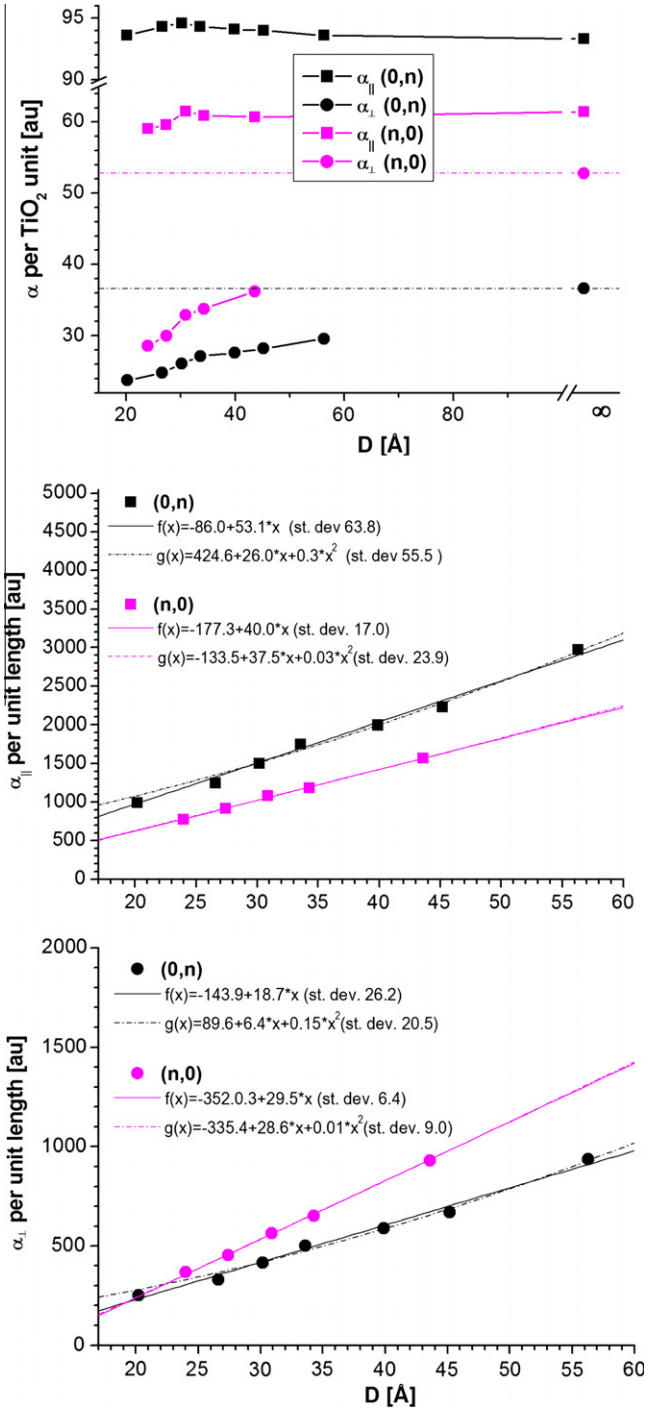

Fig. 2. Dependence of LNTs polarizabilities on the diameter D of the tubes: polarizability per TiO_2 unit (top panel), polarizability per unit length (central and bottom panel). The dotted horizontal lines represent the limit at infinite diameter.

tubes for which the dielectric response to the applied field yields an attenuation of the field inside the tube characterized by a screening factor of 2.08 for BN [26] and 4.4 for both metallic and semiconducting C tubes [27–29].

The relation between the applied field and the response field (inside the tubes) along the same transverse direction is given by classic electrostatics (the depolarization factor is 2π in this transverse z-direction; see Ref. [30]):

$$F_z^{ins} = \frac{2F_z^{out}}{1+\varepsilon_{zz}} \tag{3}$$

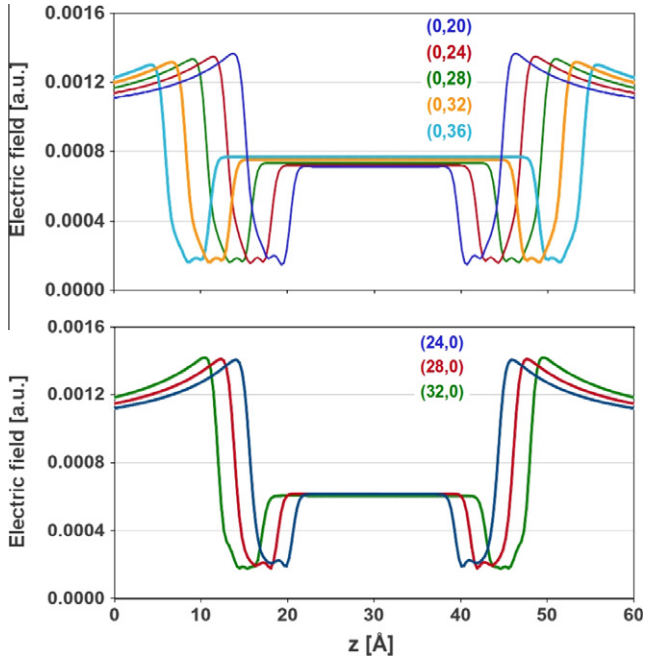

Fig. 3. The electric field along the line parallel to the z axis and going through the center of the LNTs. The applied electric field is 0.001 au.

The transverse component of the field inside the tubes depends on ε_{zz}, which is related to the volume V of the tube, given the CPKS α_{zz} values by the following expression (see Ref. [27]):

$$\begin{cases} \varepsilon_{zz} = 1 + \frac{4\pi\alpha_{zz}}{V} \\ \varepsilon_{xx} = 1 + \frac{4\pi\alpha_{xx}}{V} \end{cases} \tag{4}$$

The volume of the cylinder ($V = \pi \cdot L \cdot R_{eff}^2$ where L is the length of the cell and R_{eff} is the effective radius of the cylinder) has been derived by combining Eqs. (3) and (4). Computed values of ε_{zz}, ε_{xx} and R_{eff} are reported in Table 4. R_{eff} appears systematically larger than R reported in Table 4, but still comparable; ε_{zz} decreases with the size of the nanotubes because the density of matter $(1/V)$ decreases (larger nanotubes contains more empty space); at large V $(R \to \infty)$, ε_{zz} approaches 1. The mean value of epsilon, $\bar{\varepsilon} \sim 2$, obtained for LNTs in this work is a value considerably smaller than for bulk anatase, ($\bar{\varepsilon} \sim 5$—6): the large difference can be partially attributed to the microscopic polarizabilities of anatase and LNTs ($\bar{\alpha} \sim 80$ and 56 bohr^3/TiO_2 for anatase and (0,48) LNT, respectively) but is principally due to the large difference in the density of matter in the two materials, see Tables S5 and 4. Notice that the attempt to use the volume of the cylindrical shell: $V = \pi L\left[(R+\frac{d}{2})^2 - (R-\frac{d}{2})^2\right]$ in Eq. (4), yields values of the thickness d in the range 10–15 Å and 7–8 Å for $(0,n)$ and $(n,0)$ LNTs, respectively, thus comparable with the radius R of the tubes, Tables 3 and 4.

Alternatively, the dielectric shell model as formulated by Lan et al., [31] correlates the attenuation of the electric field inside a cylindrical shell of thickness d to the dielectric constant ε through the relation: $\frac{F_z^{out}}{F_z^{ins}} = \frac{(\varepsilon+1)^2\left(R+\frac{d}{2}\right)^2 - (\varepsilon-1)^2\left(R-\frac{d}{2}\right)^2}{4\varepsilon\left(R+\frac{d}{2}\right)^2}$. In the case of $(0,n)$ LNTs, a best fit procedure yields d = 12 Å and ε = 3.6 (st. dev. 0.014) while d = 8.2 Å and ε = 4.4 are obtained for $(0,n)$ tubes. The thickness varies a lot from a kind of tubes to the other, and the dielectric constants are larger than those obtained from Eq. (3). Nevertheless, it is interesting to notice that the expression of the ratio between the inside and outside fields given above tends to one when R is going to infinity ($d \ll R$), whatever the couple (d,ε) is: then, for very

Table 3
Properties of lepidocrocite nanotubes: diameter (D) in Angström (Å), strain energy (E_S) per TiO_2 unit in electronvolt (eV), energy gap(E_g) in electronvolt (eV), polarizability (α) in au per TiO_2 unit which are equivalent to 1.649E−41 (C^2m^2)/J, second hyperpolarizability (γ) in au per TiO_2 unit which are equivalent to 6.235E−65 (C^4m^4)/J^3. For symmetry reasons $\alpha_{yy} = \alpha_{zz}$, $\gamma_{yyyy} = \gamma_{zzzz} = 3\gamma_{yyzz}$. $\bar{\alpha} = \frac{\alpha_{xx}+2\alpha_{zz}}{3}$ and $\bar{\gamma} = \frac{1}{5}(\gamma_{xxxx} + 2\gamma_{yyyy} + 4\gamma_{xxyy} + 2\gamma_{yyzz})$. Calculations at the PBE0/A1//PBE0/A1 level with $T = (7,7,7,35,70)$ and $S = 12$. See text for details.

	(0,16)	(0,20)	(0,24)	(0,28)	(0,32)	(0,36)	(0,48)	∞	(24,0)	(28,0)	(32,0)	(36,0)	(48,0)	∞
D	20.2	24.6	30.2	33.6	39.9	45.2	56.3	∞	24.0	27.4	30.9	34.3	43.6	∞
R (=D/2)	10.1	12.3	15.1	16.8	20.0	22.6	28.2	∞	12.0	13.7	15.5	17.2	21.8	∞
E_S	0.3	0.2	0.2	0.1	0.1	0.1	0.04	0	0.6	0.5	0.4	0.3	0.2	0
E_g^{dir}	6.1	5.7	5.3	5.3	5.1	5.1	5.1	5.5	5.9	5.7	5.3	5.2	5.3	5.5
E_g^{ind}	5.7	5.5	–	–	–	–	–	–	5.8	5.6	5.2	–	–	–
α_{xx} ($\alpha^{\parallel}$)	93.6	94.3	94.6	94.6	94.1	94.0	93.6	93.4	59.1	59.6	62.5	60.9	60.7	61.4
α_{yy} ($\alpha^{\perp}$)	23.8	24.8	26.1	27.1	27.6	28.2	29.6	37.0	28.6	30.0	32.9	33.8	36.2	53.0
$\bar{\alpha}$	47.1	48.0	48.9	49.6	49.8	50.1	50.9	55.8	38.8	39.9	42.8	42.8	44.8	55.8
γ_{xxxx}	–	−3454	−6212	−7158	−7478	–	–	−7863	73,168	77,878	77,262	–	–	76,087
$\gamma_{xxyy} = \gamma_{xxzz}$	–	1082	879	836	807	–	–	504	1286	1123	412	–	–	51
$\gamma_{yyyy} = \gamma_{zzzz} = 3\ \gamma_{yyzz}$	–	3964	4567	5408	6257	–	–	28,953	2205	2492	1707	–	–	−1850
$\bar{\gamma}$	–	2289	1897	2121	2487	–	–	14,272	16,838	17,803	16,692			14,272

Table 4
Dielectric constant and third order susceptibility (atomic units) of TiO_2 nanotubes, computed according (4) and (5). S is the screening factor $\frac{F_z^{out}}{F_z^{ins}}$; R_{eff} in Å is the effective radius as derived from $V = \pi L R_{eff}^2$; d in Å is the thickness of a cylinder shell derived from $V = \pi L\left[(R+\frac{d}{2})^2 - (R-\frac{d}{2})^2\right]$; $\bar{\varepsilon} = \frac{\varepsilon_{xx}+2\varepsilon_{zz}}{3}$ and $\bar{\chi}^{(3)} = \frac{1}{5}(\chi^{(3)}_{xxxx} + 2\chi^{(3)}_{yyyy} + 4\chi^{(3)}_{xxyy} + 2\chi^{(3)}_{yyzz})$ are the mean dielectric constant and third order susceptibility, respectively. See text for details.

	(0,20)	(0,24)	(0,28)	(0,32)	(0,36)	(24,0)	(28,0)	(32,0)
S	1.40	1.39	1.36	1.33	1.30	1.63	1.62	1.65
R_{eff}	15.8	18.0	20.5	23.2	26.0	13.2	14.7	16.0
d	10.2	10.8	12.6	13.4	15.0	7.2	7.8	8.2
ε_{xx}	4.0	3.8	3.5	3.2	3.0	3.6	3.5	3.5
ε_{zz}	1.8	1.8	1.7	1.7	1.6	2.3	2.2	2.3
$\bar{\varepsilon}$	2.5	2.4	2.3	2.2	2.1	2.7	2.7	2.7
$\chi^{(3)}_{xxxx}$	−18.4	−30.4	−31.6	−29.5	–	533.6	535.2	509.4
$\chi^{(3)}_{xxyy} = \chi^{(3)}_{xxzz}$	5.8	4.4	3.6	3.2	–	9.4	7.8	2.8
$\chi^{(3)}_{xxyy} = \chi^{(3)}_{zzzz} = 3\chi^{(3)}_{yyzz}$	21.2	22.4	23.8	24.7	–	16.0	17.2	11.2
$\bar{\chi}^{(3)}$	12.2	9.3	9.4	9.8	–	122.8	122.3	110.0

large tubes, there is no more screening factor which means also that the dielectric constant is equal to one as expected from Eqs. (3) and (4).

Components of the fourth rank hyperpolarizability tensor exhibit a noticeable dependence on D, Table 3. However, while the pure periodic components converge rapidly to the infinity diameter limit, all other components converge much more slowly, in agreement with what is reported in the case of BN tubes [32]. Indeed, in the case of (0,32) and (32,0) LNTs, γ_{xxxx} differs by less than 2% with respect to the corresponding limit value, whereas large differences are reported for γ components involving at least one non-periodic direction. Although the dependence of γ on D does not exhibit a linear behaviour, at least in the diameter range of the explored LNTs (Fig. 4), it is possible to underline some general trends: γ_{xxxx} increases and γ_{xxyy} decreases with D in both $(0,n)$ and $(n,0)$ LNTs whereas γ_{yyyy} shows a different behaviour in LNTs of different morphology. Despite a certain degree of regularity in their trends, γ tensors exhibit large anisotropy and a huge dependence on tube chirality. For instance, in $(n,0)$ LNTs, the largest component is along the periodic direction (γ_{xxxx}). This component is more than 40 times as large as γ_{yyyy}. In $(0,n)$ LNTs, γ_{xxxx} is small, even negative, and the largest components of the tensor are those involving non-periodic directions: γ_{yyyy} is larger than γ_{xxxx} by a factor of 2 that increases to a factor of 5 at the infinite diameter limit according to the component values obtained for the monolayer (see Eq. (2)). This huge difference in the hyperpolarizability components due to chirality comes from the large anisotropy of the hyperpolarizability of the lepidocrocite flat sheet (see γ_{xxxx} and γ_{yyyy} component values of the slab). This latter one is probably due to the large difference between the cell parameters, $a = 3.77$ Å and $b = 3.01$ Å, of the lepidocrocite monolayer. Notice in addition, that hyperpolarizabilities are normally much more sensitive to structural differences than are polarizabilities.It is evident that, according to the formula for gamma with positive and negative contributions to its definition (see Ref. [33]), it is difficult to draw

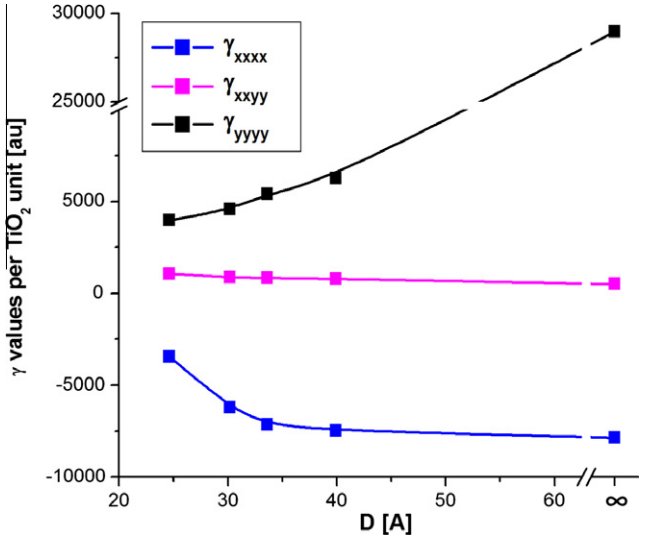

Fig. 4. Dependence of $(0,n)$ LNTs second hyperpolarizabilities on the diameter D of the tubes.

conclusion about the trend of each component or ascertain their value without doing accurate ab initio calculation. However, the mean value of gamma, $\bar{\gamma}$, at the infinite diameter limit is the same for both $(n,0)$ and $(0,n)$ tubes. Since this is not the case for tubes with D close to 30 Å, it must be because convergence with respect to D is still not reached.

The third order susceptibility components $\chi(3)_{yyyy} = \chi(3)_{zzzz}$ and $\chi(3)_{yyzz}$ have been obtained through the following formulae:

$$\begin{cases} \chi^{(3)}_{yyyy} = \frac{2\pi\gamma_{yyyy}}{3V} \\ \chi^{(3)}_{yyzz} = \frac{2\pi\gamma_{yyzz}}{3V} \end{cases} \quad (5)$$

and reported in Table 4 together with the mean values $\bar{\chi}^{(3)}$. A large dependence of $\chi^{(3)}$ values on the morphology of the tubes, at least for the size of the LNTs analyzed in this work, can be underlined. In particular $\bar{\chi}^{(3)}$ differs by one order of magnitude between $(0,n)$ and $(n,0)$ LNTs, Table 4. From bulk anatase for which a value of $\bar{\chi}^{(3)} = 3.4\text{E}-13$ esu (at 1064 nm) has been reported [34], $\bar{\gamma} = 20,352$ au/TiO_2 has been derived that compares well with $\bar{\gamma} = 14,272$ au/TiO_2 computed for LNTs, Table 3.

4. Conclusions

In conclusion, the coupled perturbed Kohn–Sham (CPKS) computational scheme used to obtain static electronic (hyper)polarizabilities of $(0,n)$ and $(n,0)$ LNTs has shown that:

(i) Longitudinal and transverse polarizabilities per unit length depend on the morphology of the tubes and exhibit an almost "linear" relationship with D that smoothly approaches the lepidocrocite monolayer values at the infinite diameter limit.
(ii) The response of the LNTs to a transverse electric field resembles the typical response of a thin dielectric shell, however it exhibits qualitative differences with respect to the behaviour of BN nanotubes. Like BN the attenuation of the field inside the tube depends on D, but unlike BN it also depends also on the chirality of the tube.
(iii) Components of the second hyperpolarizability tensor exhibit a large anisotropy and a huge dependence on the tube size and chirality. Even the infinite diameter limit of each components is unique. The trend cannot be drawn by any approach less sophisticated than accurate ab initio calculations.

Acknowledgement

The authors thank CINECA for granting access to supercomputing resources (ISCRA Award 2010).

Appendix A. Supplementary material

Supplementary data associated with this article can be found, in the online version, at http://dx.doi.org/10.1016/j.commatsci.2012.11.002.

References

[1] D.V. Bavykin, J.M. Friedrich, F.C. Walsh, Adv. Mater. 18 (2006) 2807.
[2] A. Fujishima, X. Zhang, D.A. Tryk, Surf. Sci. Rep. 63 (2008) 515.
[3] M. Ni, M.K.H. Leung, D.Y.C. Leung, Renew. Sust. Energy Rev. 11 (2007) 40.
[4] Z. Tang, Y. Ji, Y. Xu, R. Xu, Z. Zhang, Z. Zhou, Sen. Lett. 6 (2008) 933–937.
[5] D. Deng, M.G. Kim, J.Y. Lee, J. Cho, J. Energy Environ. Sci. 2 (2009) 818–837.
[6] Z.V. Saponjic, N.M. Dimitrijevic, D.M. Tiede, A.J. Goshe, X. Zuo, L.X. Chen, A.S. Barnard, P. Zapol, R. Curtiss, T. Rajh, Adv. Mater. 17 (2005) 965–971.
[7] Y.Q. Wang, G.Q. Hu, X.F. Duan, H.L. Sun, Q.K. Xue, Chem. Phys. Lett. 365 (2002) 427–431.
[8] T. Akita, M. Okumura, K. Tanaka, K. Ohkuma, M. Kohyama, T. Koyanagi, M. Date, S. Tsubota, M. Haruta, Surf. Interface Anal. 37 (2005) 265–269.
[9] A. Vittadini, M. Casarin, Theor. Chem. Acc. 120 (2008) 551–556.
[10] A.M. Ferrari, M. Lessio, D. Szieberth, L. Maschio, J. Phys. Chem. C 114 (2010) 21219–21225.
[11] D. Szieberth, A.M. Ferrari, Y. Noel, M. Ferrabone, Nanoscale 2 (2011) 81.
[12] D. Szieberth, A.M. Ferrari, P. D'Arco, R. Orlando, Nanoscale 3 (2011) 1113–1119.
[13] A.M. Ferrari, D. Szieberth, Y. Noel, Mater. Chem. 21 (2011) 4568.
[14] P. Roy, D. Kim, K. Lee, E. Spiecker, P. Schmuki, Nanoscale 2 (2010) 45.
[15] R. Dovesi, V.R. Saunders, C. Roetti, R. Orlando, C.M. Zicovich-Wilson, F. Pascale, B. Civalleri, K. Doll, N.M. Harrison, I.J. Bush, P. D'Arco, M. Llunell, CRYSTAL09, CRYSTAL09 User's Manual, University of Torino, Torino, 2009.
[16] R. Orlando, V. Lacivita, R. Bast, K. Ruud, J. Chem. Phys. 132 (2010) 244106.
[17] R. Orlando, M. Ferrero, M. Rérat, B. Kirtman, R. Dovesi, J. Chem. Phys. 131 (2009) 184105.
[18] http://www.crystal.unito.it/Basis_Sets/Ptable.html.
[19] P.J. Hay, W.R. Wadt, J. Chem. Phys. 82 (1985) 270–273.
[20] http://www.turbomole.de.
[21] C. Adamo, V. Barone, J. Chem. Phys. 110 (1999) 6158–6170.
[22] H. Sato, K. Ono, T. Sasaki, A. Tamagishi, J. Phys. Chem. B 107 (2003) 9824.
[23] Z. Benkova, I. Černušák, P. Zahradník, Int. J. Quantum Chem. 107 (2007) 2133.
[24] T. Pluta, A.J. Sadlej, J. Chem. Phys. 114 (2001) 136.
[25] M. Pecul, F. Pawłowski, P. Jørgensen, A. Köhn, C. Hättig, J. Chem. Phys. 124 (2006) 114101.
[26] G.Y. Guo, S. Ishibashi, T. Tamura, K. Terakura, Phys. Rev. B 75 (2007) 245403.
[27] R. Demichelis, Y. Noël, P. D'Arco, M. Rérat, C. Zicovich-Wilson, R. Dovesi, J. Phys. Chem. C 115 (2011) 8876.
[28] B. Kozinsky, N. Marzari, Phys. Rev. Lett. 96 (2006) 166801.
[29] W. Lu, D. Wang, L. Chen, Nanoletters 7 (2007) 2729.
[30] C. Kittel, Introduction to Solid State Physics, Wiley and Sons, Inc., New York, 1968.
[31] H.P. Lan, L.H. Ye, S. Zhang, L.M. Peng, Appl. Phys. Lett. 94 (2009) 183110.
[32] R. Orlando, R. Bast, K. Ruud, U. Ekström, M. Ferrabone, B. Kirtman, R. Dovesi, J. Phys. Chem. A 115 (2011) 12631–12637.
[33] B.J. Orr, J.F. Ward, Mol. Phys. 20 (1970) 513.
[34] S. Kumar Das, C. Schwanke, A. Pfuch, W. Seeber, M. Bock, G. Steinmeyer, T. Elsaesser, R. Grunwald, Opt. Express 19 (2011) 16985.